NASA/TP-2015-218994

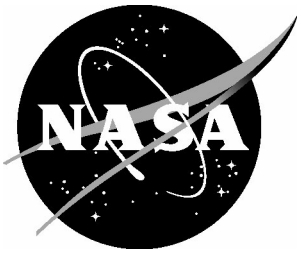

Solar Proton Transport within an ICRU Sphere Surrounded by a Complex Shield: Ray-Trace Geometry

Tony C. Slaba
Langley Research Center, Hampton, Virginia

John W. Wilson
Old Dominion University, Norfolk, Virginia

Francis F. Badavi
Old Dominion University, Norfolk, Virginia

Brandon D. Reddell, Amir A. Bahadori
Johnson Space Center, Houston, Texas

December 2015

NASA STI Program . . . in Profile

Since its founding, NASA has been dedicated to the advancement of aeronautics and space science. The NASA scientific and technical information (STI) program plays a key part in helping NASA maintain this important role.

The NASA STI program operates under the auspices of the Agency Chief Information Officer. It collects, organizes, provides for archiving, and disseminates NASA's STI. The NASA STI program provides access to the NTRS Registered and its public interface, the NASA Technical Reports Server, thus providing one of the largest collections of aeronautical and space science STI in the world. Results are published in both non-NASA channels and by NASA in the NASA STI Report Series, which includes the following report types:

- TECHNICAL PUBLICATION. Reports of completed research or a major significant phase of research that present the results of NASA Programs and include extensive data or theoretical analysis. Includes compilations of significant scientific and technical data and information deemed to be of continuing reference value. NASA counter-part of peer-reviewed formal professional papers but has less stringent limitations on manuscript length and extent of graphic presentations.

- TECHNICAL MEMORANDUM. Scientific and technical findings that are preliminary or of specialized interest, e.g., quick release reports, working papers, and bibliographies that contain minimal annotation. Does not contain extensive analysis.

- CONTRACTOR REPORT. Scientific and technical findings by NASA-sponsored contractors and grantees.

- CONFERENCE PUBLICATION. Collected papers from scientific and technical conferences, symposia, seminars, or other meetings sponsored or co-sponsored by NASA.

- SPECIAL PUBLICATION. Scientific, technical, or historical information from NASA programs, projects, and missions, often concerned with subjects having substantial public interest.

- TECHNICAL TRANSLATION. English-language translations of foreign scientific and technical material pertinent to NASA's mission.

Specialized services also include organizing and publishing research results, distributing specialized research announcements and feeds, providing information desk and personal search support, and enabling data exchange services.

For more information about the NASA STI program, see the following:

- Access the NASA STI program home page at http://www.sti.nasa.gov

- E-mail your question to help@sti.nasa.gov

- Phone the NASA STI Information Desk at 757-864-9658

- Write to:
  NASA STI Information Desk
  Mail Stop 148
  NASA Langley Research Center
  Hampton, VA 23681-2199

NASA/TP-2015-218994

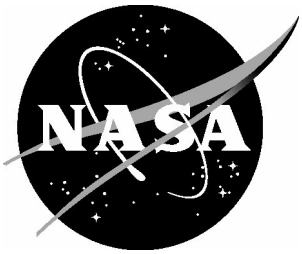

Solar Proton Transport within an ICRU Sphere Surrounded by a Complex Shield: Ray-Trace Geometry

Tony C. Slaba
Langley Research Center, Hampton, Virginia

John W. Wilson
Old Dominion University, Norfolk, Virginia

Francis F. Badavi
Old Dominion University, Norfolk, Virginia

Brandon D. Reddell, Amir A. Bahadori
Johnson Space Center, Houston, Texas

National Aeronautics and
Space Administration

Langley Research Center
Hampton, Virginia 23681-2199

December 2015

Available from:

NASA STI Program / Mail Stop 148
NASA Langley Research Center
Hampton, VA 23681-2199
Fax: 757-864-6500

Contents

Figures

Tables

Abstract

A computationally efficient 3DHZETRN code with enhanced neutron and light ion ($Z \leq 2$) propagation was recently developed for complex, inhomogeneous shield geometry described by combinatorial objects. Comparisons were made between 3DHZETRN results and Monte Carlo (MC) simulations at locations within the combinatorial geometry, and it was shown that 3DHZETRN agrees with the MC codes to the extent they agree with each other. In the present report, the 3DHZETRN code is extended to enable analysis in ray-trace geometry. This latest extension enables the code to be used within current engineering design practices utilizing fully detailed vehicle and habitat geometries. Through convergence testing, it is shown that fidelity in an actual shield geometry can be maintained in the discrete ray-trace description by systematically increasing the number of discrete rays used. It is also shown that this fidelity is carried into transport procedures and resulting exposure quantities without sacrificing computational efficiency.

Introduction

Primarily due to its high computational efficiency, the HZETRN code has been widely used throughout vehicle and habitat shield optimization activities, from preliminary architecture and trade studies through final design [Wilson et al. 2004a,b; Qualls et al. 2001; Shavers et al. 2004] and as one element of multidisciplinary optimization software [Wilson et al. 2003]. Further applications have been found in space environmental monitoring and validation [Hugger et al. 2003; Slaba et al. 2011a, 2013] and as a fundamental part of astronaut risk estimation for radiation safety monitoring [Cucinotta et al. 2008, 2013]. Despite the broad applicability, one limitation of the HZETRN model is the use of the straight-ahead approximation wherein all particles are assumed to travel along a common axis. This approximation is known to be inaccurate for low energy neutrons and light ions ($Z \leq 2$) produced at broad angles relative to the incoming primary radiation.

Three-dimensional (3D) corrections to the HZETRN formalism for neutrons and light ions have recently been implemented, resulting in the 3DHZETRN code [Wilson et al. 2014, 2015a,b]. These improved transport procedures have been compared to state of the art Monte Carlo (MC) codes, Geant4 [Agostinelli et al. 2003], FLUKA [Fasso et al. 2005, Battistoni et al. 2007] and PHITS [Sato et al. 2006, 2013], using both simplified spherical geometry [Wilson et al. 2014, 2015a] and more complex combinatorial geometry configurations [Wilson et al. 2015b]. In these benchmarks, it was generally concluded that 3DHZETRN agrees with the MC codes to the extent they agree with each other.

The 3DHZETRN code currently allows the improved transport procedures to be evaluated within general combinatorial geometry that may be defined in terms of solid objects (spheres, boxes, cylinders, ellipsoids) with unlimited nesting (i.e. objects within other objects). This capability was tested against MC simulations by considering a cylindrical outer shield with six internal objects, including a tissue sphere [Wilson et al. 2015b]. Comparisons again showed that 3DHZETRN was in good agreement with the MC codes without sacrificing computational efficiency even in the more complex geometry considered.

In principle, the current capabilities of 3DHZETRN would support the broad range of design studies and risk assessment applications discussed at the beginning of this section. However, using only a limited set of combinatorial solids to describe realistic and highly complex vehicle designs, such as the International Space Station, with thousands of internal parts would likely lead to unnecessary approximations and related errors in the geometric definitions. An alternative is to directly consider complex vehicle geometric descriptions typically developed in computer aided design (CAD) or finite element method (FEM) frameworks using ray-tracing methods. In such calculations, a ray-trace is performed over a large number of rays emanating from a target point within the geometry and extending outwards towards the exterior boundary. Along each ray, the length and type of each material traversed is stored. The resulting distribution of thicknesses is often referred to as a vehicle ray-trace or thickness distribution. Within the straight-ahead approximation of HZETRN, dosimetric quantities are quickly evaluated at the target point using either interpolation [Wilson et al. 1997] or ray-by-ray methods [Slaba et al. 2011b] coupled to the ray-trace geometry. A major advantage of this approach is that shield design is allowed to evolve in a more suitable CAD or FEM environment, instead of in the generally more restricted geometric definitions allowed by either MC transport codes or 3DHZETRN. In this work, the 3DHZETRN code is extended to allow evaluation within geometries defined simply by a vehicle thickness distribution file, referred to herein as a ray-trace geometry definition. This extension allows 3DHZETRN to be easily interfaced with methods based on CAD or FEM models that are already in common engineering practice. No modifications to the transport formalism

are required for this extension of code capability. Only the ray-tracer used within 3DHZETRN along specific transport stream directions [Wilson et al. 2014] was modified.

To test this new capability, the combinatorial geometry studied previously by Wilson et al. [2015b] will be replaced by the corresponding ray-trace geometry definition evaluated at different target point locations. Convergence tests are performed on the number of rays used in the thickness distribution to evaluate the associated geometric discretization error. It is shown that more precise geometric representations and transport code solutions are achieved as the number of rays in the thickness distribution is increased, and the current practice of using ~10^3 rays may be sufficient in some cases. Results generated with 3DHZETRN from the ray-trace geometry are compared to 3DHZETRN results and MC simulations generated in the original combinatorial geometry [Wilson et al. 2015b]. It is found that neither transport code accuracy nor efficiency is sacrificed with the extension to ray-trace geometry. This latest transport code advancement directly enables the use of more complex geometric models so that simple mapping of the present methodology into more realistic applications is achieved.

3D Transport through Ray-trace Geometry

In this section, the ray-tracer used in 3DHZETRN to estimate material types and thicknesses traversed through a ray-trace geometry definition is described. The transport formalism previously described by Wilson et al. [2014, 2015a,b] is not altered. Fig. 1 shows a case in which the external radiation environment is assumed to impinge uniformly along the direction $\boldsymbol{\Omega}_0$ onto the geometry, and the solution is being evaluated at the point $\boldsymbol{x}$ along the stream direction $\boldsymbol{\Omega}$. Transport procedures require rapid evaluation of the materials and thicknesses traversed along an arbitrary direction extending from any point within the geometry to the outer boundary (along $-\boldsymbol{\Omega}_0$ from $\boldsymbol{x}_0$ in this example). Combinatorial geometry allows this evaluation to be performed analytically in closed form as described by Wilson et al. [2015b]. In ray-trace geometry, the exact geometry specifications are replaced with a discrete set of unit ray directions, $\boldsymbol{r}_i$, emanating from $\boldsymbol{x}$, along which only the thickness, $t_i^{(j)}$, and material types traversed by the ray are known. The superscript (j) is used here to denote that in complex geometry, there may be many distinct material types, appearing along a given ray, i.

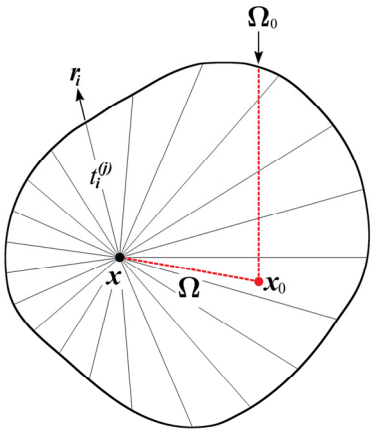

Fig. 1. General ray-trace geometry in which 3D transport procedures are evaluated.

In order to efficiently evaluate traversed materials and thicknesses through ray-trace geometry, some requirements need to be defined. First, to enable rapid searching through the distribution of rays used to define the ray-trace geometry, it is required that these rays be generated according to a latitude-longitude grid, as shown in Fig. 2. By using typical spherical coordinate transformations, the polar (longitude) and azimuthal (latitude) angles for each ray may be uniquely determined. The right side of Fig. 2 shows that these angles form a rectangular grid of points in two-dimensional space fully compatible with simple and efficient search algorithms used in bivariate interpolation. For an arbitrary ray-direction, its four nearest neighbors in the underlying ray distributions are easily found by simple search algorithms in two-dimensional space instead of computationally expensive comparisons against all ray directions in 3D space.

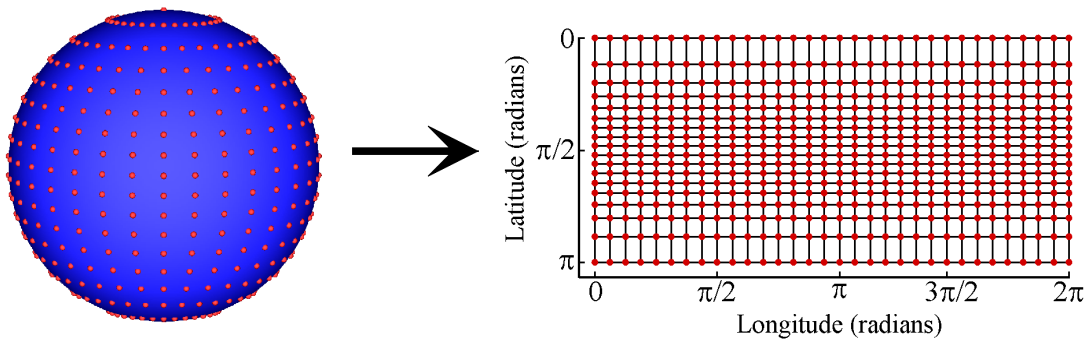

Fig. 2. Latitude-longitude distribution of rays mapped onto unit sphere (left) and onto two dimensional grid of polar and azimuthal angles (right).

The only other requirement placed on the ray-trace evaluation mode is that at least one direction vector in the ray distribution must line up exactly with the incident direction of the incoming radiation environment, $\boldsymbol{\Omega}_0$. This requirement is implicitly required in existing engineering design practice already coupled to HZETRN in the straight-ahead approximation. The main reason for including this requirement in the ray-trace mode of 3DHZETRN is to ensure that evaluation of the forward flux component along $\boldsymbol{\Omega}_0$, which can dominate the overall exposure in many cases, is performed with precise geometric definition obtained directly from the native CAD or FEM geometry.

After satisfying these computational requirements, the ray-trace procedure carried out within 3DHZETRN over the ray-trace geometry is relatively simple. Consider the problem of ray-tracing from a point $\boldsymbol{x}_1$ along a direction $-\boldsymbol{\Omega}_0$, as shown in Fig. 3. To begin, the ray direction, $\boldsymbol{v}_1$ (green dashed line in figure) connecting $\boldsymbol{x}_1$ to $\boldsymbol{x}$ is constructed and the polar and azimuthal angles for $\boldsymbol{v}_1$ are computed. The four nearest neighbors of $\boldsymbol{v}_1$ in the underlying ray distribution are then determined by quickly searching the 2D grid of values shown in Fig. 2. In the 2D plot of Fig. 3, the visible neighbors are shown as blue solid lines. The closest of the neighbors, $\boldsymbol{r}_c$, is then selected, and the material type at a distance of $d_1 = |\boldsymbol{v}_1|$ along $\boldsymbol{r}_c$ is obtained directly from the ray-trace geometry file. This material type is assigned to the point $\boldsymbol{x}_1$. A step of 0.1 mm is then taken in the direction of $-\boldsymbol{\Omega}_0$ to define a new point, $\boldsymbol{x}_2$, and the process is repeated to determine the material type for point $\boldsymbol{x}_2$.

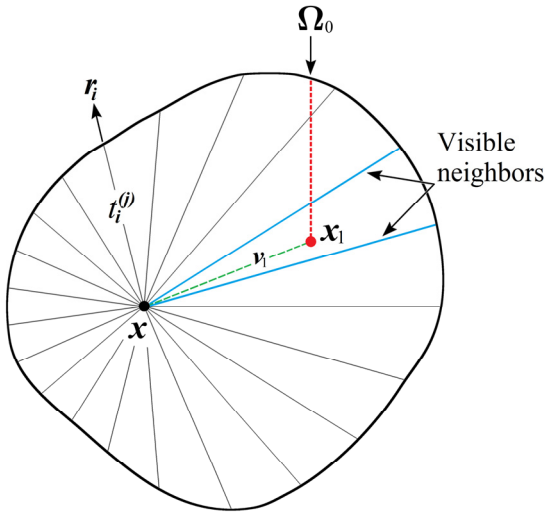

Fig. 3. Ray-trace from a point $\boldsymbol{x}_1$ in the geometry along $-\boldsymbol{\Omega}_0$.

This process is repeated until the distance $d_n = |\boldsymbol{v}_n|$, where $\boldsymbol{v}_n$ is the ray connecting $\boldsymbol{x}_n$ to $\boldsymbol{x}$, and $\boldsymbol{x}_n$ is the point associated with step n in this procedure, is larger than the known distance along the nearest neighbor. This indicates that the outer boundary of the geometry has been reached. The end result of this procedure is a list of $\boldsymbol{n}$ material

types corresponding to points spaced 0.1 mm part in the geometry along the ray direction $-\mathbf{\Omega}_0$. Adjacent steps with identical material types are collapsed into a single step, so that the final information returned to the transport procedures is a list of contiguous material layers extending from the point of interest to the outer boundary in the specified direction. In the following section, various convergence tests are performed to evaluate functionality and accuracy of the described procedure.

Inhomogeneous Geometry

In this section, various convergence tests and comparisons are performed to test the ray-trace geometry mode of 3DHZETRN. In these tests, the combinatorial geometry of Wilson et al. [2015b], shown in Fig. 4, was ray-traced to generate the thickness distributions needed as input into the transport code. A precise definition of the original combinatorial geometry definition follows, but it should be understood that the analysis presented in this section is for transport code results using the ray-trace geometry definition derived from the combinatorial geometry.

Fig. 4 shows a 30 cm diameter tissue equivalent sphere [ICRU 1993] placed within a 2.47 cm (5 g/cm^2) thick cylindrical aluminum shell (outer diameter 75 cm, outer length 175 cm) with 4.9 cm (10 g/cm^2) thick end caps. In addition to the International Commission on Radiation Units and Measurements (ICRU) sphere at the center of the aluminum cylindrical shell, an interior aluminum box with dimensions 46.3×14.8×14.8 cm (upper right corner in Fig. 4) and a second aluminum box with dimensions 22.2×22.2×37.0 cm (lower left corner in Fig. 4) are also placed inside the cylinder. The dimensions of these boxes in units of g/cm^2 are 125×40×40 and 60×60×100, respectively. Target points (detectors) are placed within the ICRU tissue sphere, similar to the studies of Wilson et al. [2014, 2015a]. The detector locations appearing at the top and bottom of the ICRU tissue sphere will be referred to in subsequent figures, tables, and discussion as $z = 0$ and $z = 30$, respectively (z is parallel to $\mathbf{\Omega}_0$). Additional target points within the ICRU tissue sphere are therefore defined by their location between the top and bottom detectors. For example, the detector location in the center of the sphere is referred to as $z = 15$.

For all calculations, the external radiation environment (external source boundary condition) is positioned above the geometry and directed uniformly downward along $\mathbf{\Omega}_0$ as indicated by the arrows in Fig. 4. The boundary condition, or external source, is the Webber representation of the February 23, 1956 solar particle event (SPE) [Webber 1966]. The Webber 1956 SPE is given by an exponential momentum spectrum with momentum parameter $p_0 = 100$ MV and 10^9 protons/cm^2 above 30 MeV.

To begin the process of testing transport procedures in ray-trace geometry, the number of rays required to adequately represent the geometry is examined. It is important to note that the convergence tests and related discussion and conclusions in this work are specific to the geometry being considered. More complex geometry would necessitate similar testing procedures to quantify the discretization error associated with representing the geometry with a finite number of rays.

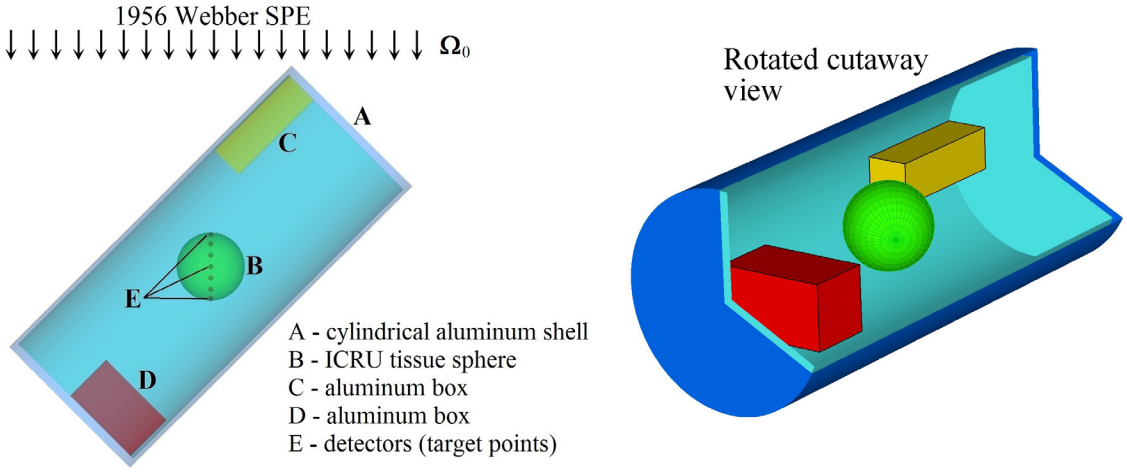

Fig. 4. Complex geometry used in the current study: ICRU tissue sphere shielded by an aluminum cylindrical shell with internal parts.

Fig. 5 gives a sequence of images showing converging geometric resolution with increasing number of rays, N_{ray}, in the original ray-trace file. These images were created by first generating a series of ray-trace files, each one corresponding to a target point placed at the center of the ICRU tissue sphere and with a different N_{ray} value. These files were then individually input into 3DHZETRN, and a large number of target points and ray directions were arbitrarily chosen. Each target point and direction was passed to the ray-tracer described in the previous section to evaluate approximate location of material interfaces. The location of the material interfaces, as determined from the internal ray-tracer, were then plotted as scatter points to create the images in Fig. 5.

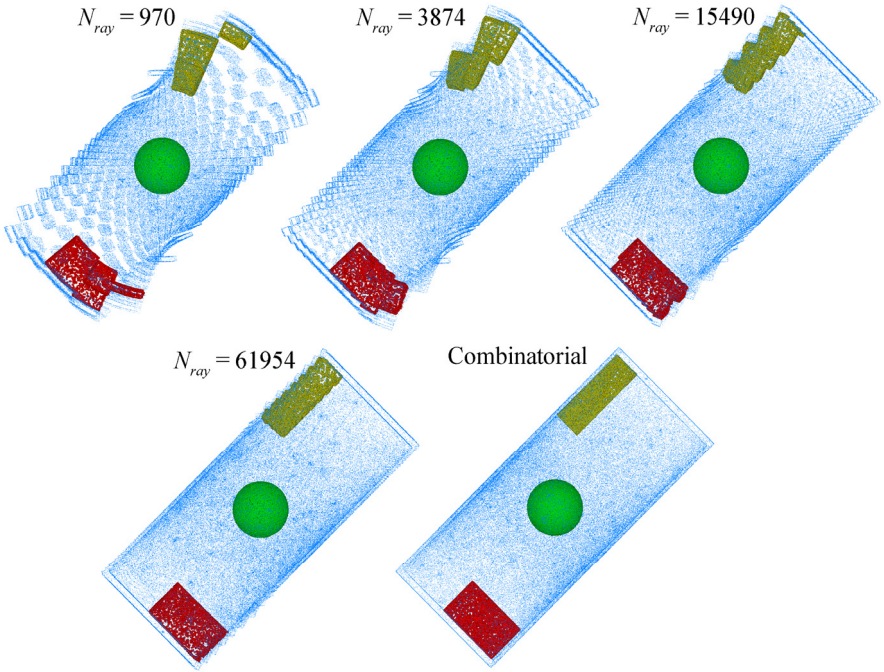

Fig. 5. Geometric representation associated with ray-trace geometry (N_{ray} = 970, 3874, 15490, 61954) and combinatorial geometry.

Two observations should be made in connection to Fig. 5. First, objects closer to the original target point at the center of the ICRU sphere at which ray-traces were evaluated are in clear focus even with a small number of rays. As the distance from the original target point increases, so too does the lateral distance between adjacent rays, leading to greater geometric distortion. If the target point used in the original ray-trace files were placed in the upper right box, for example, greater distortion would occur in the ICRU sphere, and the upper right box would be in clearer focus regardless of the chosen N_{ray} value. Second, although considerable geometric distortion occurs for the lower number of rays, the geometric representation is seen to systematically focus at the larger number of rays, indicating that a converging sequence of transport solutions should be expected for increasing N_{ray} values.

An important point to keep in mind is that the geometric distortion shown in Fig. 5 only impacts the isotropic components of the neutron and light ion spectra. By requirement, as noted in the previous section, the forward component of the transport solution is evaluated directly over a ray for which exact material and thickness information from the original geometry is known, and no approximate ray-trace methods are utilized. In many cases, the forward component of the flux dominates the overall exposure, so that total exposure quantities and fluence spectra would be expected to be reasonably accurate. Moreover, geometry distortion far from the target point of interest, as shown in Fig. 5, will necessarily lead to errors in the spatial distribution of isotropic neutron source terms driving 3D transport procedures. This can be seen in Fig. 6, where the integral isotropic neutron source induced within the geometry by the Webber 1956 SPE is plotted. The source terms far from the evaluation point play less of a role in determining the isotropic neutron and light fluence spectra than the source terms very near the evaluation point, for which geometric distortion is minimal. This also indicates that the distortion shown in Figs. 5 and 6 may not cause substantial error in the induced particle spectra within the geometry. Still, the impact of this apparent geometric distortion on the isotropic components of the neutron and light ion spectra needs to be further investigated.

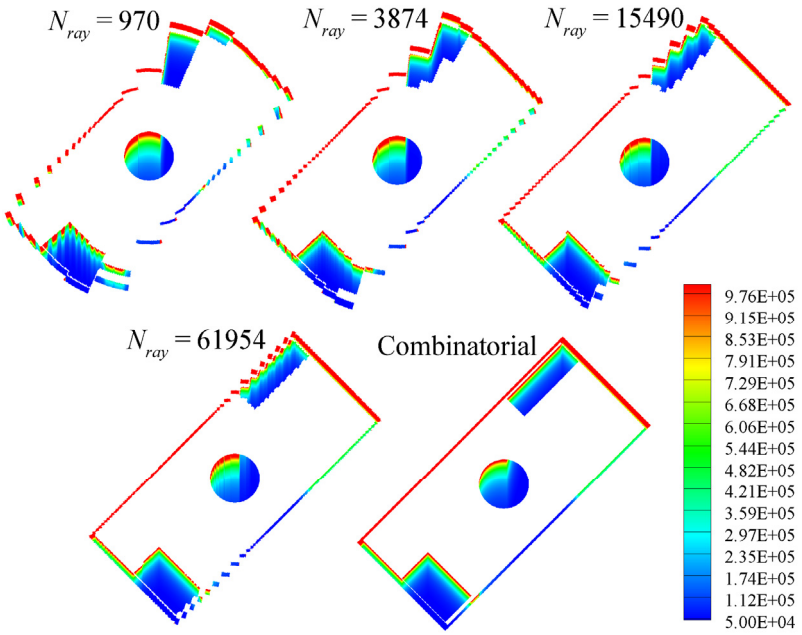

Fig. 6. Integral ($E > 1$ MeV) isotropic neutron source (particles/(g-event)) induced by the Webber SPE using ray-trace geometry (N_{ray} = 970, 3874, 15490, 61954) and combinatorial geometry.

The effect of geometry discretization on radiation field quantities is now examined. Wilson et al. [2015b] previously established that $N = 26$ transport streams are required to evaluate the radiation fields in the combinatorial geometry being considered presently. Although results are not shown here, it has been verified that $N = 26$ transport streams are adequate in the corresponding ray-trace geometry as well, and results given in subsequent tables and figures were all generated with $N = 26$ transport stream directions. Of greater interest is the number of rays required in the ray-trace geometry file to adequately describe the actual geometry. Figs. 5 and 6 have already provided some indication of preliminary requirements, and now dosimetric quantities and fluence spectra are evaluated to provide quantitative assessments.

Fluence spectra evaluated for various N_{ray} values are shown in Fig. 7, and dose and dose equivalent results are given in Tables 1 and 2. Despite the geometry and neutron source distortions seen in Figs. 5 and 6, fluence spectra are nearly identical with results appearing as overlapping on the log-log scale plot of Fig. 7.

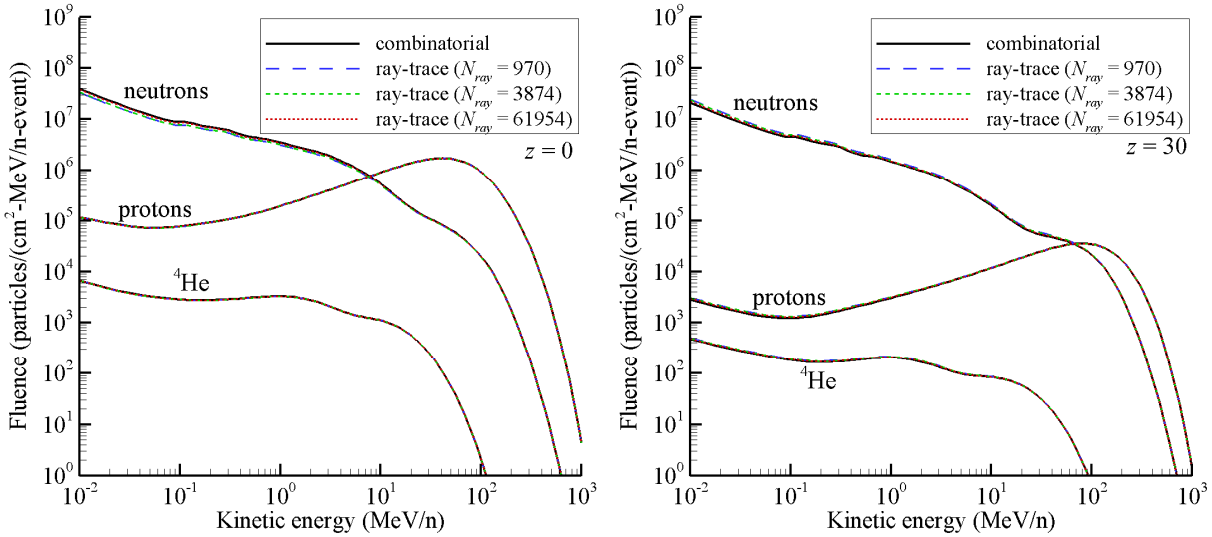

Fig. 7. Fluence spectra evaluated at the top (left) and bottom (right) of the ICRU sphere for both combinatorial representation and ray-trace geometry approximation.

Table 1. Dose at points in tissue sphere for various N_{ray} values used in ray-trace geometry. Results from Wilson et al. [2015b] for the combinatorial geometry are also provided for comparison.

z (g/cm^2)	Dose (cGy/event)				
	N_{ray} = 970	N_{ray} = 3874	N_{ray} = 15490	N_{ray} = 61954	Combinatorial
0	42.78	42.78	42.79	42.79	42.79
0.007	42.48	42.48	42.48	42.48	42.49
0.3	38.74	38.74	38.75	38.75	38.75
1	32.38	32.38	32.39	32.39	32.39
5	14.59	14.60	14.60	14.60	14.59
25	1.55	1.55	1.55	1.55	1.55
29	1.13	1.13	1.13	1.13	1.13
29.7	1.08	1.08	1.08	1.08	1.07
29.993	1.05	1.05	1.05	1.05	1.05
30	1.04	1.04	1.04	1.04	1.04

Table 2. Dose equivalent at points in tissue sphere for various N_{ray} values used in ray-trace geometry. Results from Wilson et al. [2015b] for the combinatorial geometry are also provided for comparison.

z (g/cm^2)	Dose Equivalent (cSv/event)				
	N_{ray} = 970	N_{ray} = 3874	N_{ray} = 15490	N_{ray} = 61954	Combinatorial
0	65.89	65.90	65.94	65.97	65.99
0.007	62.39	62.40	62.45	62.48	62.51
0.3	55.22	55.24	55.30	55.33	55.36
1	46.03	46.04	46.10	46.12	46.15
5	20.78	20.81	20.82	20.82	20.81
25	2.62	2.61	2.60	2.59	2.59
29	2.08	2.07	2.06	2.06	2.04
29.7	2.03	2.01	2.00	2.00	1.98
29.993	1.99	1.97	1.96	1.96	1.94
30	1.90	1.89	1.87	1.87	1.85

Slight discrepancies can be seen in the neutron spectra below 10 MeV/n and are quantified in Fig. 8 where the relative difference between the neutron spectra obtained in the combinatorial geometry and various ray-trace geometries are plotted. Relative differences for other light ions were found to be smaller than what is shown in Fig. 8 for neutrons. It can be seen that relative differences are within $\pm$20% across the full energy range and diminish with increasing N_{ray} values. Relative differences are also reduced at the highest energies where the forward component of the flux dominates the solution, and geometric distortion shown in Fig. 6 has negligible impact.

In Table 1, it is found that dose converges quickly with increasing N_{ray}, and only negligible differences are found between results derived from ray-trace and combinatorial geometry descriptions. Dose equivalent values derived from the ray-trace geometry are only a few percent different than the values obtained within the more detailed combinatorial geometry. The slightly larger variation observed for dose equivalent is attributed to errors in the low energy light ion fluence spectra as shown in Fig. 7.

These errors can be more clearly seen in Fig. 9, where the alpha fluence from Fig. 7 has been shown on an expanded scale. The low energy alpha fluence at z = 30 shows very slight systematic errors as a function of the N_{ray} value. It can be seen that the largest N_{ray} value of 61954 yields results almost identical (within 2%) to the combinatorial geometry results, suggesting that even small-scale detail in the particle fluence spectra found at evaluation points near material interfaces can be captured within the ray-trace geometry, provided that enough rays are used.

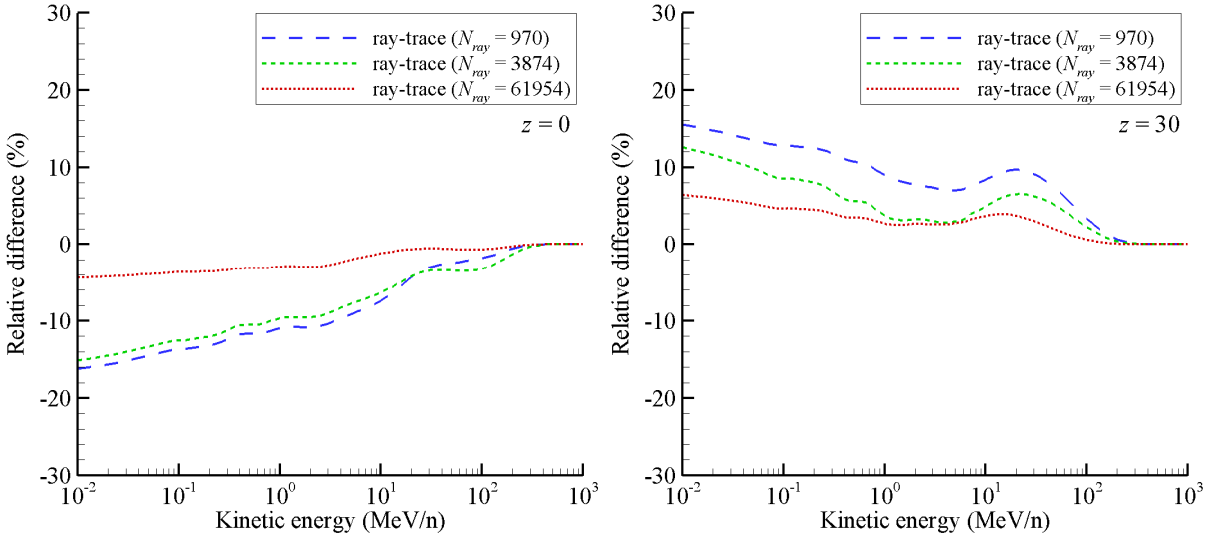

Fig. 8. Relative difference (%) between neutron spectra from Fig. 7 obtained in combinatorial geometry and various ray-trace geometries.

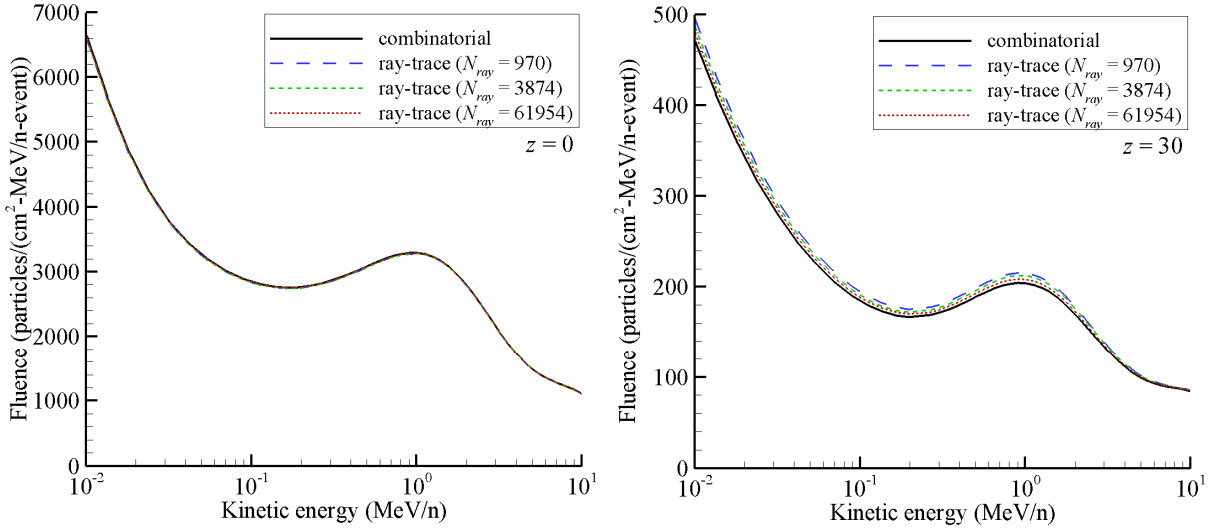

Fig. 9. Alpha fluence from Fig. 7 with vertical axis in linear scale to improve clarity.

It is encouraging that the differences associated with varying N_{ray} show little effect on the spectra, dose, and dose equivalent and that computational efficiency has been maintained in the ray-trace geometry mode, as indicated in Table 3. Fig. 10 gives a final comparison between MC results and 3DHZETRN in combinatorial mode [Wilson et al. 2015b] along with new results in ray-trace mode with N_{ray} = 61954. The ray-trace derived results are clearly in good agreement with the MC simulations and with the combinatorial results. It can also be seen that variation amongst the MC codes, associated almost entirely with differing nuclear interaction models, greatly exceeds the variation associated with various N_{ray} values used in 3DHZETRN in ray-trace mode, as shown in Fig. 7. This indicates that the geometric distortion associated with ray-trace geometry definitions leads to transport model errors that are much smaller than current uncertainties in the underlying nuclear physics models used in the codes.

Table 3. Total CPU time required for transport calculations.

Code	Combinatorial	N_{ray} = 970	N_{ray} = 3874	N_{ray} = 15490	N_{ray} = 61954
CPU time (sec)	59	66	68	71	83

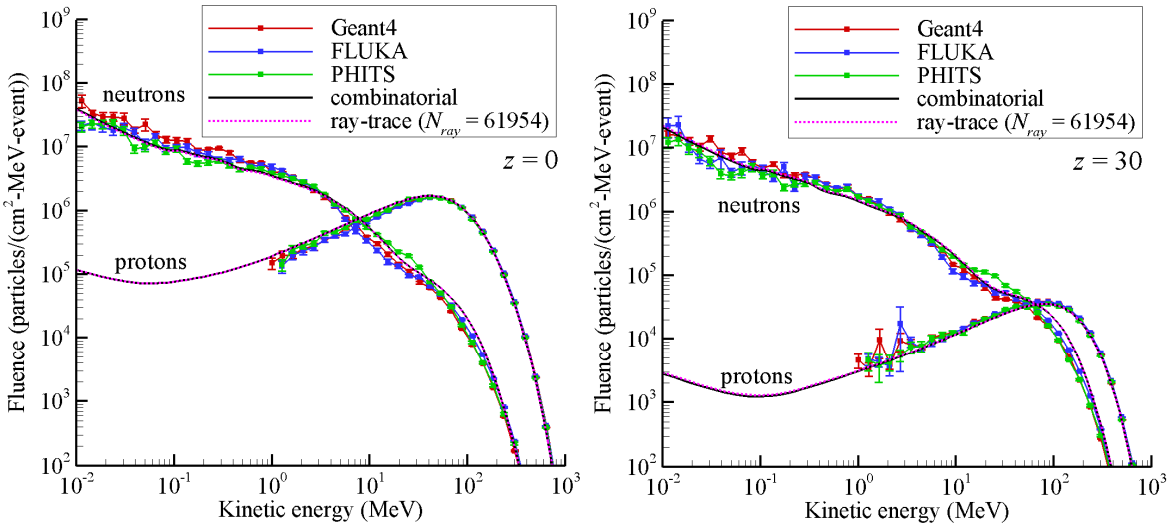

Fig. 10. Fluence spectra evaluated at the top (left) and bottom (right) of the ICRU sphere for both combinatorial representation and ray-trace geometry approximation compared to MC simulations.

Summary

In this work, extensions to the 3DHZETRN code were presented, allowing the code to be evaluated in ray-trace geometry. This latest update enables the code to be coupled to highly detailed vehicle and habitat designs that are commonly developed, maintained, and optimized in CAD or FEM environments. All that is needed for the coupling between 3DHZETRN and fully detailed geometry is the generation of a single thickness distribution through ray-tracing procedures already implemented in current engineering design practice. Minimal requirements are imposed to enable efficient coupling and were described. These requirements allow efficient look-up procedures to be carried out within 3DHZETRN over the ray-trace geometry and are actually consistent with current requirements already in use with HZETRN in the straight-ahead approximation.

To test the updated transport code, the combinatorial geometry of a prior study [Wilson et al. 2015b] was considered, and convergence tests were performed. These tests revealed that increasing the number of rays used in the underlying ray-trace geometry description sufficiently reduced geometric discretization error and spatial distortion of the isotropic neutron source term. Transported exposure quantities such as dose, dose equivalent, and fluence were also examined to quantify error associated with reducing precise combinatorial geometry to discrete ray-trace representations. It was shown that both dose and dose equivalent values can be precisely calculated in the ray-trace geometry with negligible error compared to values derived from the exact combinatorial geometry. Comparisons to previous MC simulations [Wilson et al. 2015b] also showed that uncertainties in the nuclear physics models greatly exceed the error associated with discrete ray-trace geometric representations, indicating that the updated code is suitable for a broad range of engineering applications at least in the context of present nuclear interaction knowledge. Clearly, an increase in fidelity of nuclear models and their validation with laboratory experiments are needed.

References

Agostinelli, S. et al., Geant4--a simulation toolkit. *Nucl. Instrum. & Methods A* **506**: 250-303; 2003.

Battistoni, G., Muraro, S., Sala, P.R., Cerutti, F., Ferrari, A., Roesler, S.,Fasso, A., Ranft, J., The FLUKA code: Description and benchmarking. *Proceedings of the Hadronic Shower Simulation Workshop 2006*, **896**: 31–49; 2007.

Cucinotta, F.A., Kim, M.Y., Willingham, V., George, K.A., Physical and biological organ dosimetry analysis for international space station astronauts. *Rad. Res.* **170**: 127–138; 2008.

Cucinotta, F.A., Kim, M.Y., Chappell, L.J., Space radiation cancer risk projections and uncertainties – 2012. NASA TP-2013-217375, 2013.

Fasso, A., Ferrari, A., Ranft, J., Sala, P.R., FLUKA: A multi-particle transport code, CERN-2005-10, INFN/TC 05/11, SLAC-R-773, 2005.

Hugger, C.P., Qualls, G.D., Wilson, J.W., Cucinotta, F.A., Shavers, M.R., Zapp, N., ISS as a platform for environmental evaluation. *AIP Conf. Proc.* **654**: 1011-1017; 2003.

ICRU, Internal Commission on Radiation Units and Measurements, Quantities and units in radiation protection dosimetry, ICRU Report 51, 1993.

Qualls, G.D., Wilson, J.W., Sandridge, C.A., Cucinotta, F.A., Nealy, J.E., Heinbockel, J.H., Hugger, C., Verhage, J., Anderson, B.M., Atwell, W., Zapp, N., Barber, R., International space station shielding model development. SAE ICES 2001-01-2370, 2001.

Sato, T., Niita, K., Iwase, H., Nakashima, H., Yamaguchi, Y., Sihver, L., 2006 Applicability of particle and heavy ion transport code PHITS to the shielding design of spacecrafts, *Rad. Meas.*, **41:** 1142 – 1146; 2006.

Sato, T., Niita, K., Matsuda, N., Hashimoto, S., Iwamoto, Y., Noda, S., Ogawa, T., Iwase, H.,Nakashima, H., Fukahori, T., Okumura, K., Kai, T., Chiba, S., Furuta T., Sihver, L., Particle and heavy ion transport code system PHITS, version 2.52, *J. Nucl. Sci. Technol.* **50**: 913-923; 2013.

Shavers, M.R., Zapp, N., Barber, R.E., Wilson, J.W., Qualls, G., Toupes, L., Ramsey, S., Vinci, V., Smith, G., Cucinotta, F.A., Implementation of ALARA radiation protection on the ISS through polyethylene shielding augmentation of the Service Module Crew Quarters, *Adv. Space Res.* **34**: 1333-1337; 2004.

Slaba, T.C., Blattnig, S.R., Badavi, F.F., Stoffle, N. N., Rutledge, R.D., Lee, K.T., Zapp, N., Dachev, T.P., Tomov, B.T., Statistical validation of HZETRN as a function of vertical cutoff rigidity using ISS measurements. *Adv. Space Res.* **47**: 600-610; 2011a.

Slaba, T.C., Blattnig, S.R., Clowdsley, M.S., Variations in lunar neutron dose estimates. *Rad. Res.* **176**: 827-841; 2011b.

Slaba, T.C., Blattnig, S.R., Reddell, B., Bahadori, A., Norman, R.B., Badavi, F.F., Pion and electromagnetic contribution to dose: Comparisons of HZETRN to Monte Carlo results and ISS data. *Adv. Space Res.* **52**: 62-78; 2013.

Webber, W.R., An evaluation of solar-cosmic-ray events during solar minimum. D2-84274-1, Boeing Co. 1966.

Wilson, J.W, Miller, J.M., Konradi, A., Cucinotta, F.A., Shielding strategies for human space exploration. NASA CP-3360, 1997.

Wilson, J.W., Korte, J.J., Sobieski, J., Badavi, F.F., Chokshi, S.M., Martinovic, Z.N., J. Cerro, J., Qualls, G.D., Radiation shielding, MDO processes, and single stage to orbit design, AIAA Space 2003, Sept 22, 2003, Long Beach, California, AIAA 2003-6259, 2003.

Wilson, J.W., Tripathi, R.K., Qualls, G.D., Cucinotta, F.A., Prael, R.E., Norbury, J.W., Heinbockel, J.H., Tweed, J., Space radiation transport methods development, *Adv. Space Res*. **34**: 1319-27; 2004a.

Wilson, J.W., Cucinotta, F.C., Schimmerling, W.S., Emerging radiation health-risk mitigation technologies. *AIP Conf. Proc.* **699**, 913-924; 2004b.

Wilson, J.W., Slaba, T.C., Badavi, F.F., Reddell, B.D., Bahadori, A.A., Advances in NASA space radiation research: 3DHZETRN, *Life Sci. Space Res.* **2**: 6-22; 2014.

Wilson, J.W., Slaba, T.C., Badavi, F.F., Reddell, B.D., Bahadori, A.A., 3DHZETRN: Shielded ICRU spherical phantom, *Life Sci. Space Res.* **4**: 46-61; 2015a.

Wilson, J.W., Slaba, T.C., Badavi, F.F., Reddell, B.D., Bahadori, A.A., Solar proton transport within an ICRU sphere surrounded by a complex shield: combinatorial geometry, NASA TP-2015-218980, 2015b.

REPORT DOCUMENTATION PAGE

Form Approved
OMB No. 0704-0188

1. REPORT DATE *(DD-MM-YYYY)*	2. REPORT TYPE	3. DATES COVERED *(From - To)*
01- 12 - 2015	Technical Publication	

4. TITLE AND SUBTITLE

Solar Proton Transport within an ICRU Sphere Surrounded by a Complex Shield: Ray-Trace Geometry

5a. CONTRACT NUMBER

5b. GRANT NUMBER

5c. PROGRAM ELEMENT NUMBER

6. AUTHOR(S)

Slaba, Tony C.; Wilson, John W.; Badavi, Francis F.; Reddell, Brandon; Bahadori, Amir A.

5d. PROJECT NUMBER

5e. TASK NUMBER

5f. WORK UNIT NUMBER

651549.02.07.10

7. PERFORMING ORGANIZATION NAME(S) AND ADDRESS(ES)

NASA Langley Research Center
Hampton, VA 23681-2199

8. PERFORMING ORGANIZATION REPORT NUMBER

L-20652

9. SPONSORING/MONITORING AGENCY NAME(S) AND ADDRESS(ES)

National Aeronautics and Space Administration
Washington, DC 20546-0001

10. SPONSOR/MONITOR'S ACRONYM(S)

NASA

11. SPONSOR/MONITOR'S REPORT NUMBER(S)

NASA/TP-2015-218994

12. DISTRIBUTION/AVAILABILITY STATEMENT

Unclassified - Unlimited
Subject Category 93
Availability: STI Program (757) 864-9658

13. SUPPLEMENTARY NOTES

14. ABSTRACT

A computationally efficient 3DHZETRN code with enhanced neutron and light ion ($Z < 2$) propagation was recently developed for complex, inhomogeneous shield geometry described by combinatorial objects. Comparisons were made between 3DHZETRN results and Monte Carlo (MC) simulations at locations within the combinatorial geometry, and it was shown that 3DHZETRN agrees with the MC codes to the extent they agree with each other. In the present report, the 3DHZETRN code is extended to enable analysis in ray-trace geometry. This latest extension enables the code to be used within current engineering design practices utilizing fully detailed vehicle and habitat geometries. Through convergence testing, it is shown that fidelity in an actual shield geometry can be maintained in the discrete ray-trace description by systematically increasing the number of discrete rays used. It is also shown that this fidelity is carried into transport procedures and resulting exposure quantities without sacrificing computational efficiency.

15. SUBJECT TERMS

3DHZETRN; HZETRN; Radiation shielding; Space radiation

16. SECURITY CLASSIFICATION OF:			17. LIMITATION OF ABSTRACT	18. NUMBER OF PAGES	19a. NAME OF RESPONSIBLE PERSON
a. REPORT	b. ABSTRACT	c. THIS PAGE			STI Help Desk (email: help@sti.nasa.gov)
					19b. TELEPHONE NUMBER *(Include area code)*
U	U	U	UU	19	(757) 864-9658